RESEARCH OF ULTRASONIC MATERIAL REMOVAL MECHANISM AT HYBRID ELECTROCHEMICAL FINISHING

Paul-Andrei Constantin[1], Paul-Mihai Pelengică[1], Constantin-Andrei Sandu[1],
Liviu-Daniel Ghiculescu[1], Cornel-Cristian Enciu[1]
[1]POLITEHNICA University of Bucharest, paulandrei001@yahoo.com, paul.mihai.pelengica@gmail.com, a_sandu45@yahoo.com, daniel.ghiculescu@upb.ro, cornel.enciu@upb.ro

ABSTRACT: This paper presents the current state of the art of ultrasonic aided electrochemical polishing, which involves anodic dissolving of the machined material predominantly around the microgeometry peaks of the machined surface, ultrasonic depassivation of the neutral layer deposited on the machined surface and roughness (Ra) decrease by ultrasonic removal of the microgeometry protrusions. Numerical simulations of ultrasonic concentrators integrating different tool sizes and different thicknesses of the electrical insulating layer to achieve the resonance condition are performed. Numerical simulations are also developed on the process of material removal and depassivation when machining a stainless steel. The results of the numerical simulations are validated by experimental results obtained, which show the correct operation of the ultrasonic chains and finding an optimum value of ultrasonic power (pressure) for maximum Ra decrease.
KEYWORDS: electrochemical polishing, ultrasonic, numerical simulation.

1. INTRODUCTION

Electrochemical Machining (ECM) is the controlled removal of (electrically conductive) material from a workpiece based on the principle of anodic dissolution according to Faraday's laws of electrolysis [1, 15, 16]. ECM is used for machining complex shapes from conductive materials, which are difficult to machine with other conventional methods [10, 11]. The process is not affected by the hardness of the material and has the following advantages: obtaining a good surface quality and a very high productivity, up to $10^5 mm^3/min$ (similar to milling) [2, 3]. During electrochemical machining in ultrasonic field (Electrochemical Machining Aided by Ultrasonics - ECM+US), ultrasonic waves create gas microbubbles on the surface of the workpiece which, by imploding, produce a large amount of energy that brings advantages on improved depassivation of the neutral layer formed on the machined surface, as well as roughness reduction by removing the peaks of the surface microgeometry [7].

2. CURRENT STATUS

In ECM polishing (or finishing), the phenomenon of anodic dissolution (figure 1), which occurs in the electrolytic medium (1) as a result of the electric field of intensity E created between the tool (2) (cathode) and the workpiece (3) (anode), has the following explanation:

- on the surface of the workpiece, the passivated layer (4) is formed, the thickness of which is smaller in the region of the micro-peaks [2, 17].

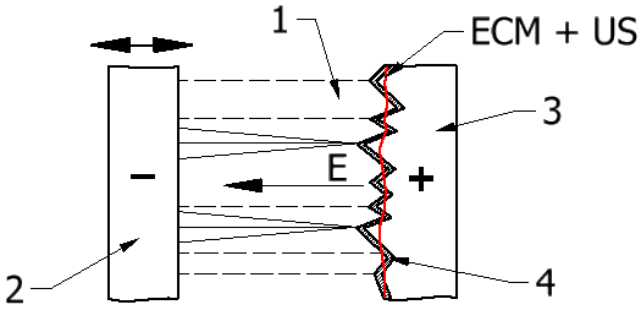

Figure 1. ECM +US polishing mechanism scheme [adapted from 2]

The oscillating movement of the tool in the ultrasonic field causes gas bubbles to form in the machining gap. By approaching the tool, they implode and produce a large amount of energy (ultrasonic cavitation).
When these micro-implosions of bubbles occur, the material is removed by reducing the peaks of the micro-geometries present on the surface of the part. A higher quality of surface and improved depassivation of the neutral layer is achieved [6, 9].
Ultrasonic assist of ECM also yields increased productivity by improving electrolyte flow through the machining gap [8]. ECM+US also brings advantages when using low energy compared to conventional ECM [12] where electrolyte pressures of 20-25 atm. are used for depassivation [4, 5].

3. ULTRASONIC CHAINS USED TO ASSIST ECM POLISHING

The construction of the ultrasonic chains is as shown in figure 2a [2]. In figure 2b can be seen the wave formation which include the transducer.

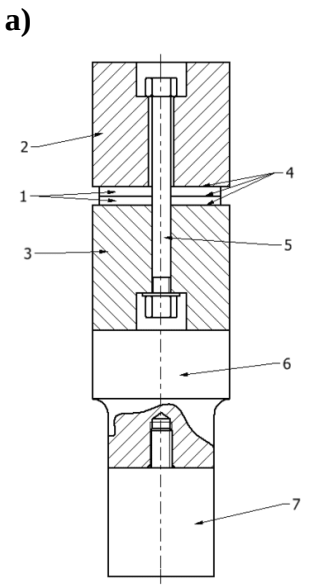

Figure 2. Ultrasonic chain and stationary wave formation [2]

The ultrasonic machining system consists of an US generator, which converts the industrial frequency of 50 Hz AC current from the main grid into an ultrasonic frequency, f_{US}=20-40KHz applied to the transducer of the ultrasonic chain - fig. 2. a, example of the construction of a US chain, used at USM, where: 1 - discs made of piezoceramic material; 2 - steel reflecting bushing; 3 - duralumin radiating bushing; 4 - 0.2...0.3 mm thick copper blades (through which the transducer is connected to the US generator); 5 - clamping screw; the pre-bending force (of tone force magnitude) is controlled so that the piezoceramic material transmits the oscillations with minimum losses; 6 - concentrator; 7 - tool, included in the US chain.

In the ultrasonic chain, standing waves are formed resulting from the superposition of elementary waves of the same frequency travelling in opposite directions, figure 2b [2]. Some points oscillate with minimum amplitude.

The ECM+US polishing surfaces for which numerical simulations were performed are shown in figures 3, 4, 5.

4. NUMERICAL SIMULATION STEPS FOR ULTRASONIC CONCENTRATOR

Simulation of the US concentrator is performed in COMSOL Multiphysics by representing the US concentrator, which integrates the tool and helps to determine the eigenfrequency. This is used to obtain the resonance condition, the operating condition of the US chain, the equilibrium between the eigenfrequency of the concentrator and the transducer. In figure 6, the model parameters are shown. In figure 7 is shown the discretization of the ultrasonic chain into free triangular finite elements. In figure 11, the boundary conditions for determining the eigenfrequency of the concentrator are shown - without mechanical constraints.

Name	Expression	Value	Description
l1	54.64[mm]	0.05464 m	Length of radiating bushing
r1	26 [mm]	0.026 m	Radius of radiating bushing
l2	60 [mm]	0.06 m	Length of concentrator
r2	15.17[mm]	0.01517 m	Radius of concentrator
densitate	7950 [kg/m^3]	7950 kg/m³	Steel Density
modulE	2.1*10^11	2.1E11	Young's Module for Steel
hscula	32[mm]	0.032 m	Length of Tool
rscula	r2	0.01517 m	Radius of Tool
hg1	10[mm]	0.01 m	Stud 1 Hole Length
rg1	4[mm]	0.004 m	Stud 1 Hole Radius
hp1	8[mm]	0.008 m	Stud 1 Length
hg2	6[mm]	0.006 m	Stud 2 Hole Length
rg2	3[mm]	0.003 m	Stud 2 Hole Radius
hp2	5[mm]	0.005 m	Stud 2 Length
roCu	8940 [kg/m^3]	8940 kg/m³	Copper Density
modulECu	1.532E11 [Pa]	1.532E11 Pa	Young's Module for Copper
gv	0.6[mm]	6E-4 m	Thickness of paint

Figure 6. Numerical simulation parameters

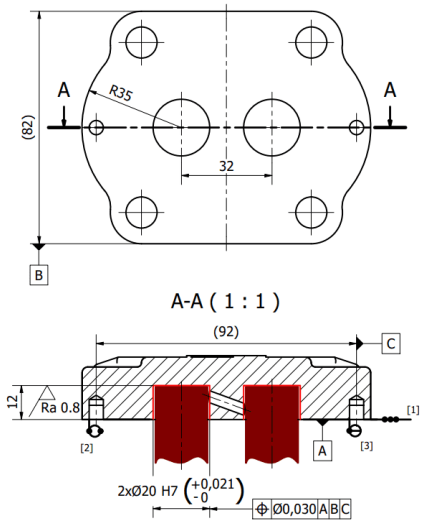

Figure 3. Operation 1

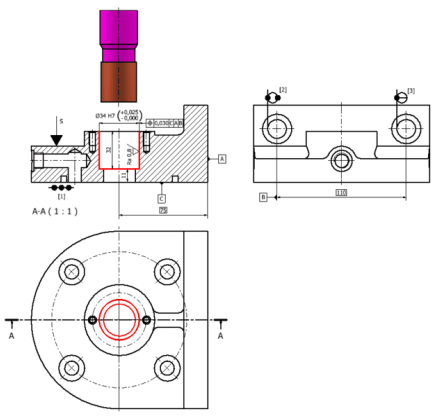

Figure 4. Operation 2

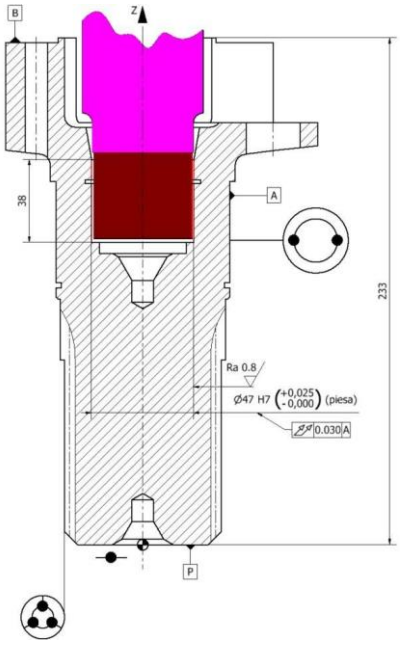

Figure 5. Operation 3

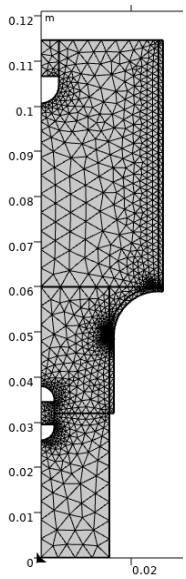

Figure 7. Discretization of the ultrasonic concentrator

The model has been assigned materials according to figures 8, 9 and 10 where the three zones of the ultrasonic chain are illustrated, the concentrator has been assigned the physical-mechanical properties of C45 (density, $\rho = 7950$ [kg/m^3], Young's modulus, $E = 2.1 \cdot 1011$ Pa, Poisson's ratio, $\nu = 0.28$), the electrode-tool of copper (density, $\rho = 8940$ [kg/m^3], Young's modulus, $E = 1.532 \cdot 1011$ Pa, Poisson's ratio, $\nu = 0.034$), and the insulation layer was assigned the properties of epoxy paint (density, $\rho = 1600$ [kg/m^3], Poisson's ratio, $\nu = 0.7$).

As the concentrator is made of a steel (C45) it is electrically conductive, so the insulation layer aims to eliminate the electric field between the tool and the workpiece on the surface not intended for machining.

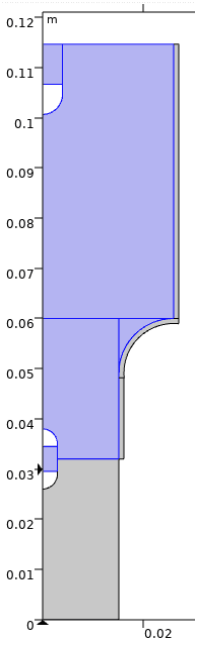

Figure 8. Concentrator, C45

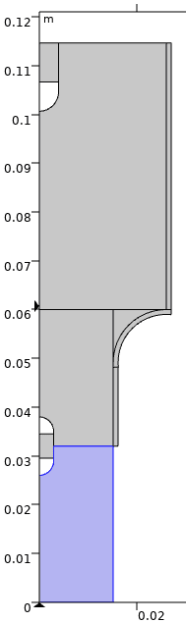

Figure 9. Electrode - tool, Cu

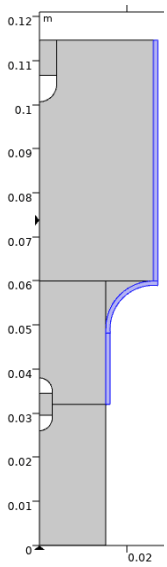

Figure 10. Isolation layer, epoxy paint

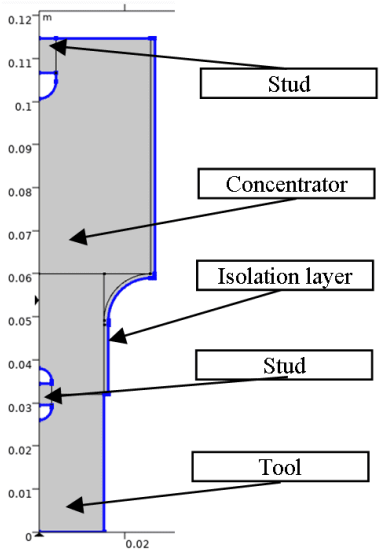

Figure 11. Boundary conditions for determining eigenfrequency

5. ANALYSIS OF RESULTS FOR THE EIGENFREQUENCY OF THE ULTRASONIC CONCENTRATOR

The simulation results provide information about the natural frequency of the ultrasonic chain. The length of the concentrator and the integrated tool will be determined in order to have at the tip of the tool a frequency of 20100 Hz which is the frequency of the transducer (target frequency) for the thickness of the 0.6 mm insulating layer (to be applied on the real concentrator).

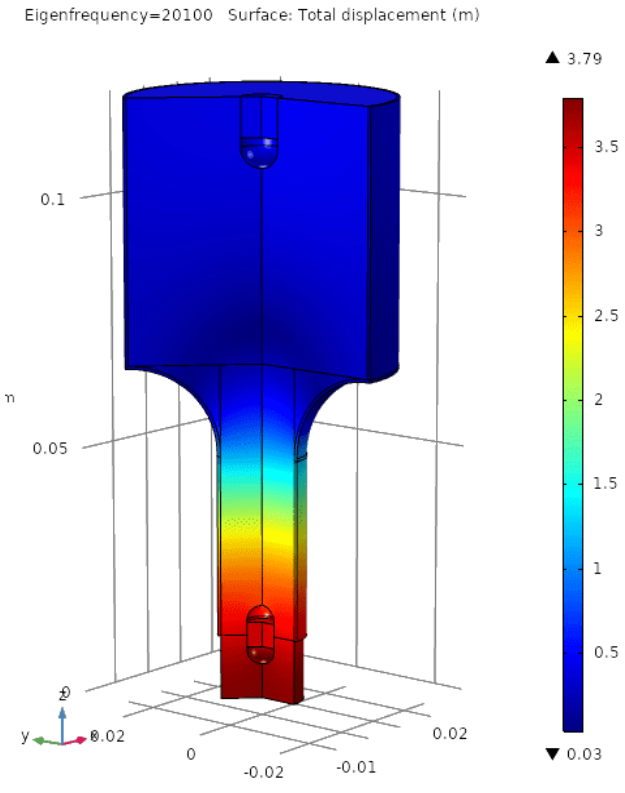

Figure 12. Tool radius = 8,17 mm

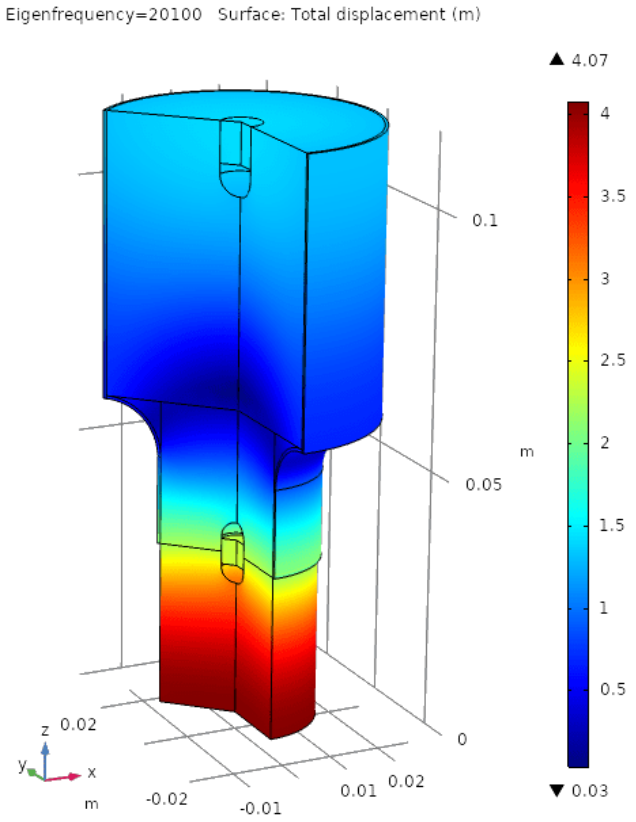

Figure 13. Tool radius = 15,17 mm

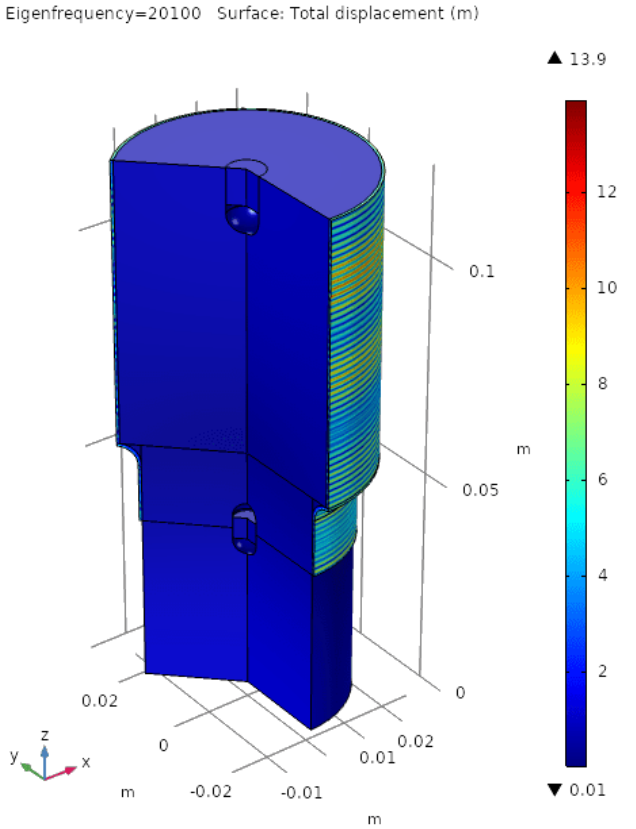

Figure 14. Tool radius = 21,67 mm

The results of the simulations are shown in figures 12, 13 and 14, these represent the three cases, where the tool parameters, radius (R) and length, vary with the surface to be machined.

After analysing the data from the first simulation it is determined how the eigenfrequency varies with the thickness of the insulating layer.

Thus, it decreased with increasing thickness of the insulating layer in the range 0.2 - 1 mm. The results are centralized in figure 15.

It can be seen that the resonant frequency, 20100 Hz, was obtained at an insulating layer thickness of 0.6 mm for all three US chains studied.

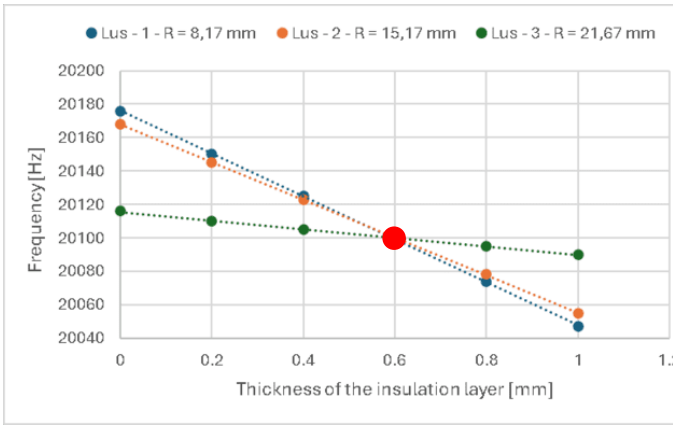

Figure 15. Eigenfrequency of the concentrator as a function of the insulating layer

6. DETERMINATION OF THE NODAL PLANE HEIGHT

In the following, the same three cases of ultrasonic chains with different tool electrode radius will be analysed to determine the nodal plane position:

- tool radius = 8.17 mm (figure 16)
- tool radius = 15.17 mm (figure 17)
- tool radius = 21.67 mm (figure 18)

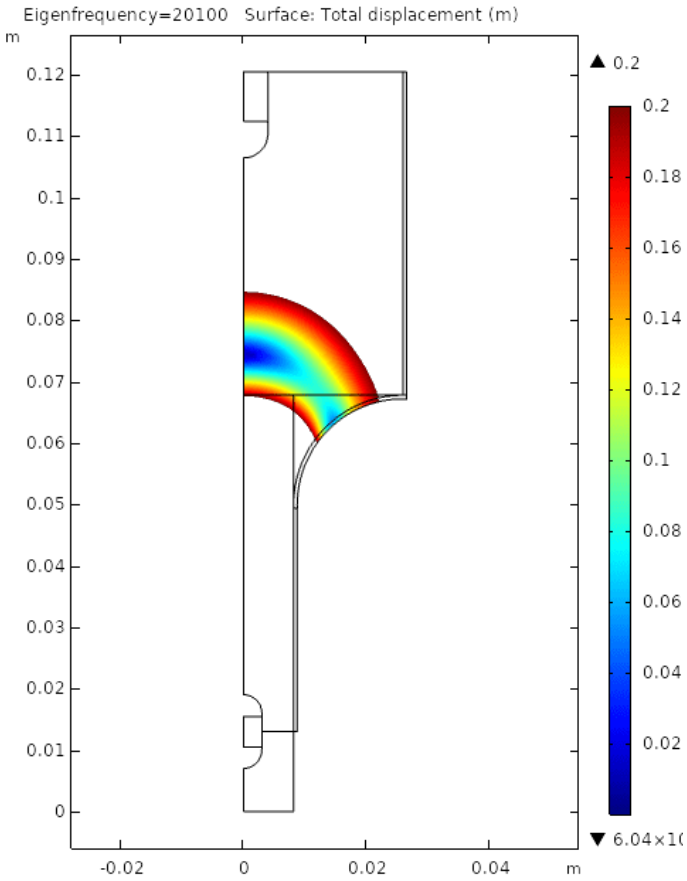

Figure 16. Tool radius = 8,17 mm

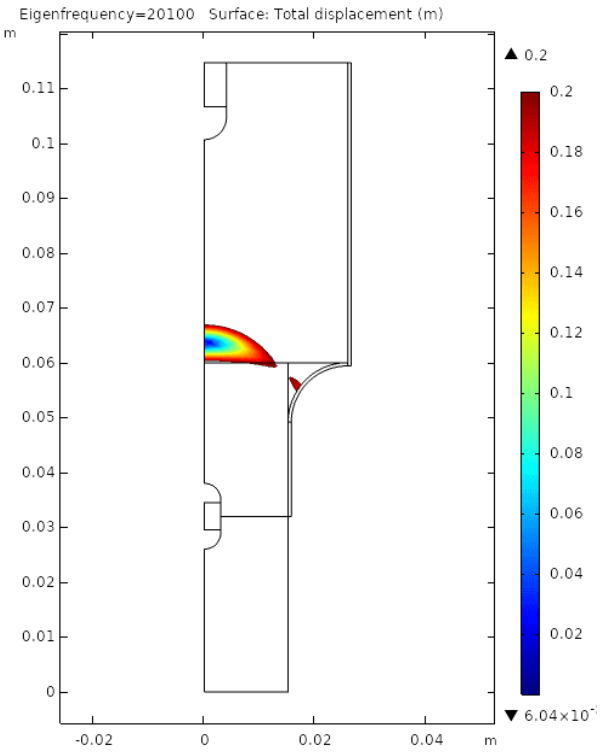

Figure 17. Tool radius = 15,17 mm

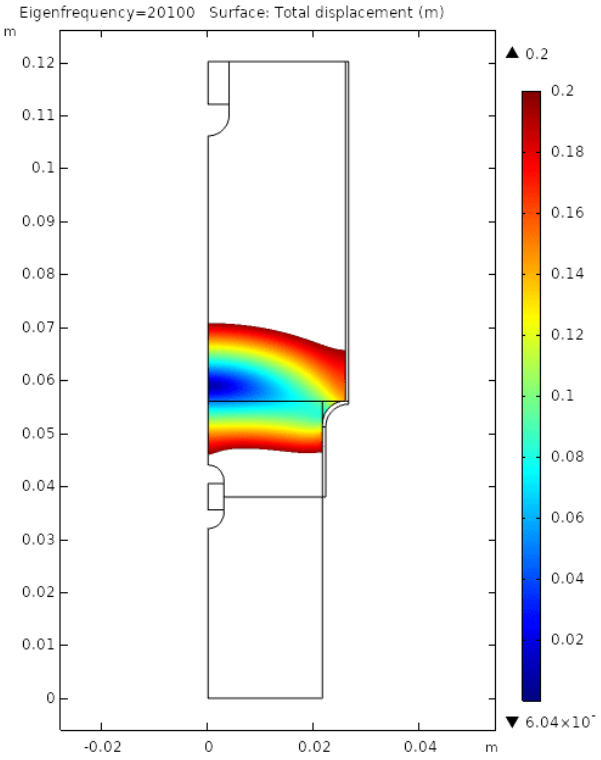

Figure 18. Tool radius = 21,67 mm

The results of the simulations are shown in table 1:

Table 1. Simulation results

Electrode radius	R = 8,17 mm	R = 15,17 mm	R = 21,67 mm
Nodal plane height	74,32 mm	63,68 mm	58,9 mm

The purpose of these simulations was to find the height at which the nodal plane is located, in order to create a nodal channel that will be used for the radial fastening of the US chain.

7. STAGES OF SIMULATED ULTRASONIC CAVITATIONS

The formation, development and collective implosion of gas bubbles as a result of ultrasonic cavitations in the machining gap is represented during a period (cycle) of ultrasonic oscillation in figure 19. It can be seen that the collective implosion of gas bubbles occurs at the end of the tool lifting half-period (stretching of the electrolytic liquid), at which time high pressures with the magnitude of 100 MPa are developed, forming directed shock waves along the machining gap, parallel to the machined surface. Implosion time is calculated to be 0.8 µs for a machining gap of 0.1 mm [2].

Numerical simulation was performed in COMSOL Multiphysics, 2D axis symmetric, in the solid mechanics module using a time-dependent study, over the time of 0.8 µs implosion. The stress produced by the bubble implosion was simulated using a contact pressure on the surface of the microdepression (SM).

In figure 20 the parameters of the model are presented. In order to achieve geometry of the piece, the materials that will be assigned to the model were taken into account, namely: at the bottom is a stainless steel (SS 41003 alloyed with 12% Cr), and an iron oxide is formed on the SM (Fe2O3) - electrically neutral layer - resulting in electrochemical processes through combining the positive ions of the part with the negative ions in the electrolyte solution.

Name	Expression	Value	Description
hp	5[mm]	0.005 m	Workpiece Hight
lp	10[mm]	0.01 m	Workpiece Length
Ra	0.636e-6	6.36E-7	Rughness before the ECM+US process
PRa	0.1[mm]	1E-4 m	Microneragularity's Pitch
pf	0.5e-6	5E-7	Thickness of the pasivated layer
tus	0.8e-6	8E-7	Cavitation bubble implosion time
modulinox	200[GPa]	2E11 Pa	Young's Module for Stainless steel
nuinox	0.29	0.29	Poisson's Ratio for Stainless Steel
tau0	313.6	313.6	Braking strength shear fatigue [MPa] C120
pus	200[MPa]	2E8 Pa	Cavitational US pressure
modulFe2O3	300[GPa]	3E11 Pa	Young's Module for iron oxide
roFe2O3	4345	4345	Density of Iron oxide
nuPFe2O3	0.24	0.24	Poisson's Ratio for Iron Oxide
tau0Fe2O2	57.6	57.6	Braking stregth shear fatigue [MPa] Iron oxide

Figure 20. Simulation parameters

In figure 21 are presented boundary and loading conditions of the model: the piece is placed on a flat surface (fixed base on the bottom surface of the model in simulation) and on the SM a pressure of contact produced by the force exerted during the implosion of gas bubbles.

Due to the small size of interstitial surface processing, the direction of these forces is horizontal, parallel to the processed surface on the sense negative of the OX axis.

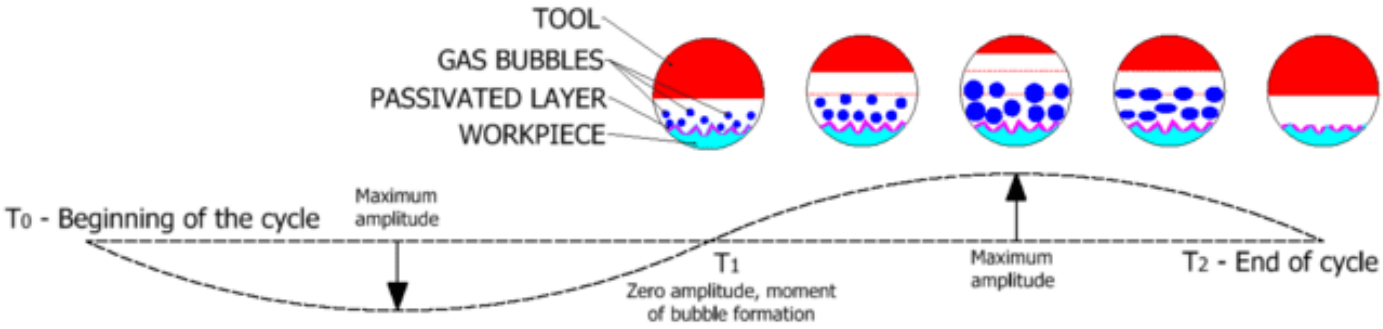

Figure 19. The implosion cycle of gas bubbles on the level of microgeometry

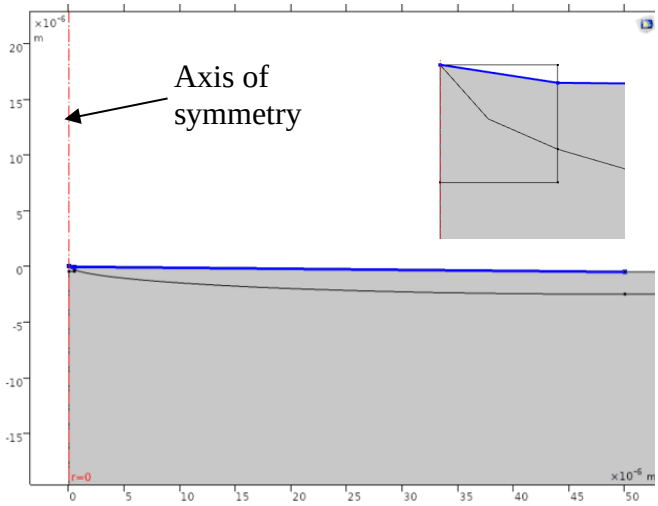

Figure 21. Simulation parameters

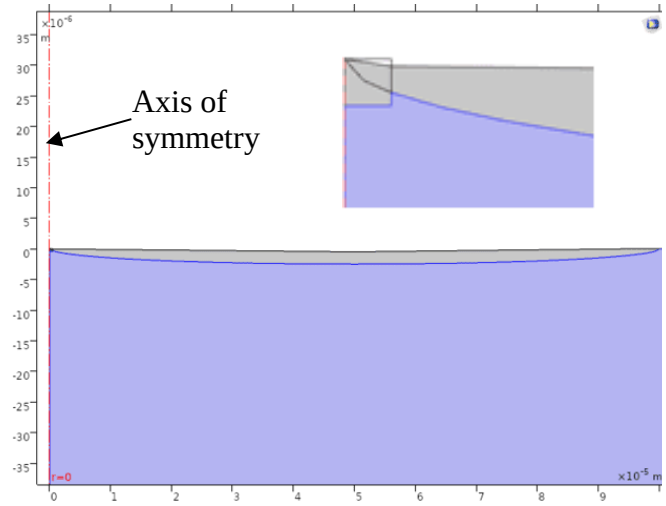

Figure 23. Stainless steel material area

The geometry of the model was created considering the distribution of iron oxide especially at the tip of the roughness as shown in figure 22 (mechanical properties of Fe2O3 are: density, $\rho = 4345$ [kg/m^3], Young's modulus, $E = 300 \cdot 1011$ Pa [14] , Poisson's ratio, $\nu = 0.24$).

Figure 23 shows how the rest of the part is made of SS 41003 with the following mechanical properties: density, $\rho = 7800$ [kg/m^3], Young's modulus, $E = 2 \cdot 1011$ Pa, Poisson's ratio, $\nu = 0{,}29$.

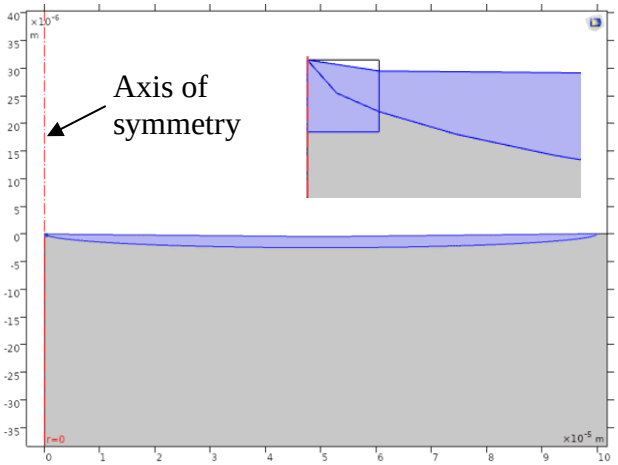

Figure 22. The area of the passive layer at the tip of the microgeometry

8. RESULTS

The following will analyse two simulation cases in which the cavitational US pressure varies.

In the first case, a relatively low pressure of 50 MPa is applied. This aims at removing the neutral layer (depassivation).

The simulation results were compared with the shear fatigue strength (τ_0) of iron oxide determined using the relations [13].

$$\tau_0 = 0{,}6 * 1{,}6 * \sigma_r \text{ [MPa]} \quad (1)$$
$$\sigma_r = 60 \text{ MPa}$$
$$\tau_0 = 0{,}6 * 1{,}6 * 60$$
$$\tau_0 = 57{,}6 \text{ MPa},$$

where, σ_r is the static breaking strength.

This highlights the area where the ultimate tensile strength is higher than the admissible one: 57.6 MPa.

These results are shown in figures 24 and 25. Therefore, these areas are removed as a result of ultrasonic cavitation.

In the second case, the cavitational US pressure is increased to 200 MPa in order to simulate the removal of the passivated layer, but also the microgeometry peaks to reduce the roughness.

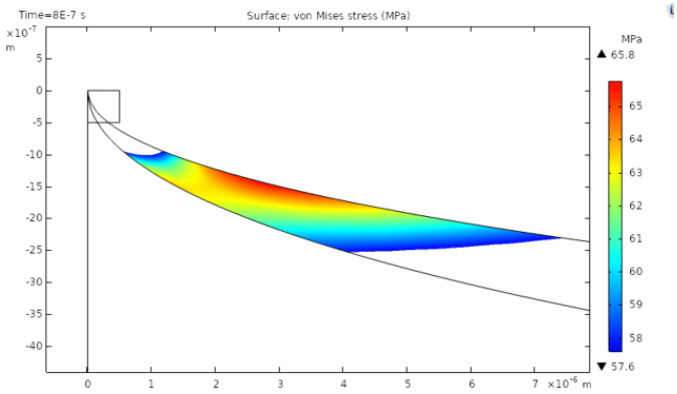

Figure 24. 2D representation of the removed material

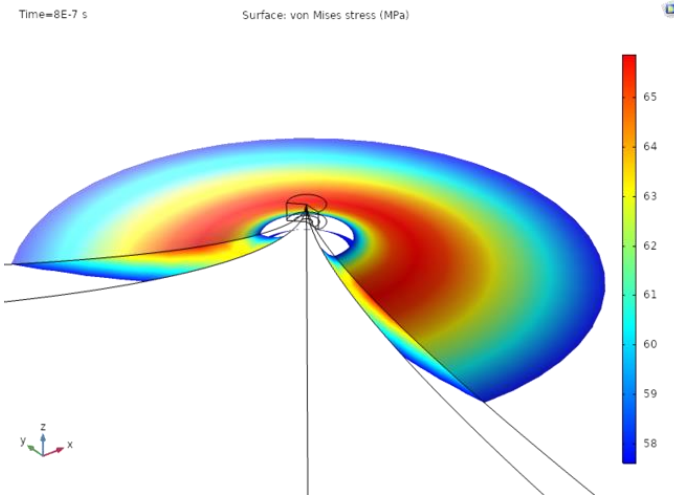

Figure 25. 3D representation of the removed material

The simulation results were compared with the fatigue shear strength of stainless steel determined with the relations [13].

$$\tau_0 = 0{,}6 * 1{,}6 * \sigma_r \text{ [MPa]} \qquad (2)$$
$$\sigma_r = 550 \text{ MPa}$$
$$\tau_0 = 0{,}6 * 1{,}6 * 550$$
$$\tau_0 = 440 \text{ MPa}$$

Thus, the points where the breaking stress is higher than the admissible one (440 MPa) are highlighted. These results can be seen in figures 26 and 27. So, these areas are removed in following implosions produced by US cavitation.

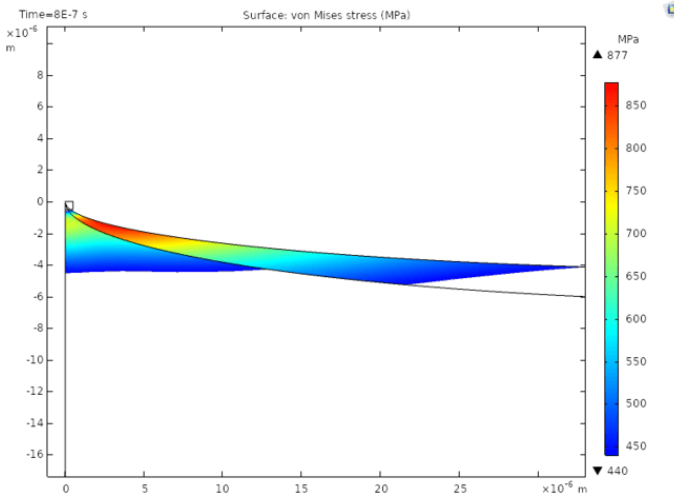

Figure 26. 2D representation of the removed material

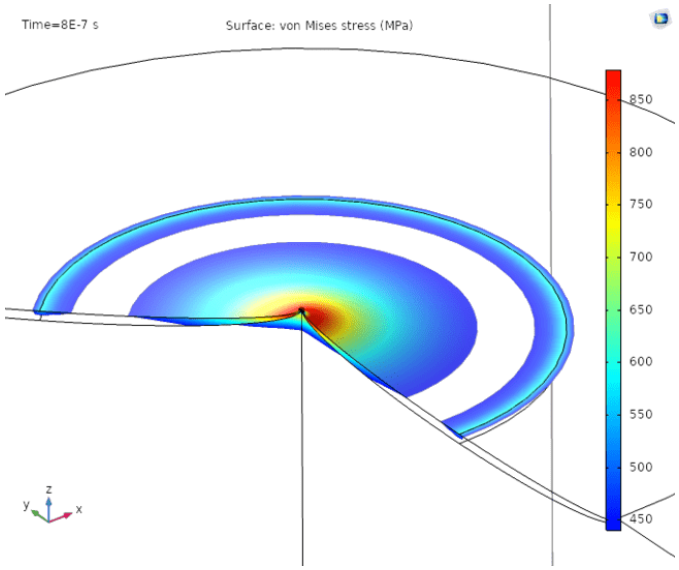

Figure 27. 3D representation of the removed material

Figure 28 shows the variation of the depth of the sampled layer depending on the ultrasonic pressure, after several runs of the model.

Thus, the pressure (which corresponds to an optimal value of the power of the US generator), so that the roughness of the processed surface is minimized.

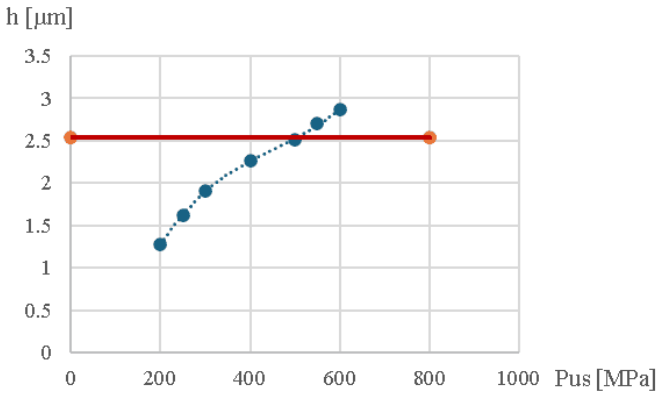

Figure 28. The influence of pressure on the processing depth

The depth of the initial microdepression (2.544 µm) was marked with the horizontal red line. Increasing the pressure results in a deeper depth of material being removed, which increases the initial roughness (Ra 0.636 µm).

This corresponds to the Ra measured on the workpiece.

9. THE STAND AND EXPERIMENTAL RESULTS

Several machining operations were performed with the values of power consumption, Pcus of the US generator, in the above-mentioned range and the experimental results are shown in the table 2. Ra values were measured with the ISR-C002 INSIZE universal roughness tester.

The experimental stand was made by dr. eng. As. C. Enciu for successive ECM+US machining.

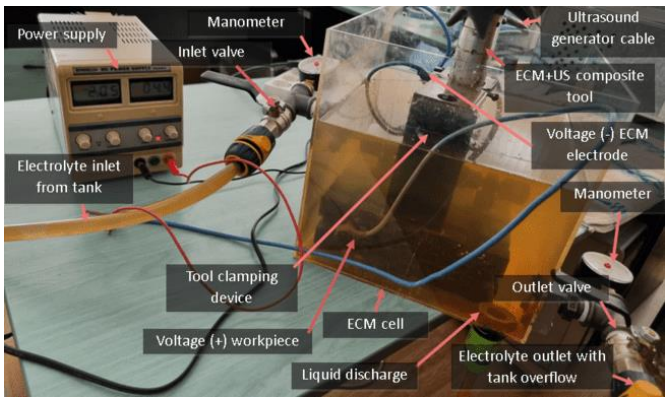

Figure 29. Experimental stand – electrolytic cell

Figure 30. ECM+US machining area

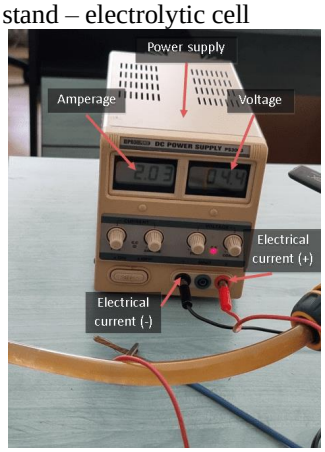

Figure 31. Power supply

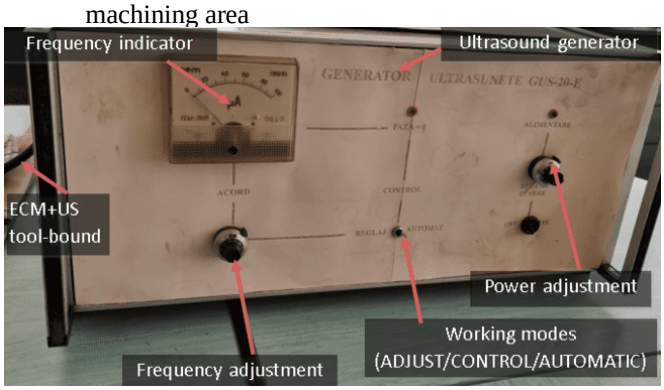

Figure 32. Ultrasound generator

The machining steps were:

- positioning and clamping the 12% Cr Stainless Steel part in the working station;
- bringing the ultrasonic concentrator into working position, frontal gap s_F=0.7 mm (fig. 30);
- starting the electrolyte tank pump;
- filling the electrolyte cell with electrolyte fluid (fig. 29);
- switching on the source and setting the working parameters (1A and 0,44 V) (fig. 31);
- ECM of a 4,9 cm^2 area, for 3 min;
- switching off the power supply;
- recirculation of electrolyte for 30s to wash the machined surface of impurities;
- switching on the US generator (fig. 32);
- generator adjustment at resonant frequency, f_0 = 20100 Hz and power consumption, Pcus = 93-119 W;
- US machining for 3 min;
- switching off the US generator;
- emptying the counterpressure chamber of electrolytic fluid;
- US chain release;
- removal of the workpiece;
- cleaning the workpiece.

Table 2. Experimental results

J = 0.25 [A/cm^2], S=4.9 cm^2		Start	End, ECM, US t=3 min	
P_{cus} [W]	I [A]	Ra [µm]	Ra [µm]	Ra reduction [%]
95	1	0.916	0.735	19.8
103	1	0.488	0.341	30.1
109	**1**	**0.636**	**0.419**	**34.1**
114	1	0.808	0.586	27.5
119	1	0.863	0.707	18.1

The graphical representation of the variation of roughness as a function of power consumption (Pcus) on the machined surface (figure 33) shows that the maximum reduction, 34% of Ra is obtained at Pcus=109 W.

A SEM QUANTA INSPECT F50 scanning electron microscope image of the machined surface (figure 34) shows a non-uniform removal of the material due to the existence of the usual (light-colored) Cr carbide particles smaller than 500 nm in the stainless steel. Cavities resulting from ultrasonic erosion are also observed, with dimensions of about 1-2 µm.

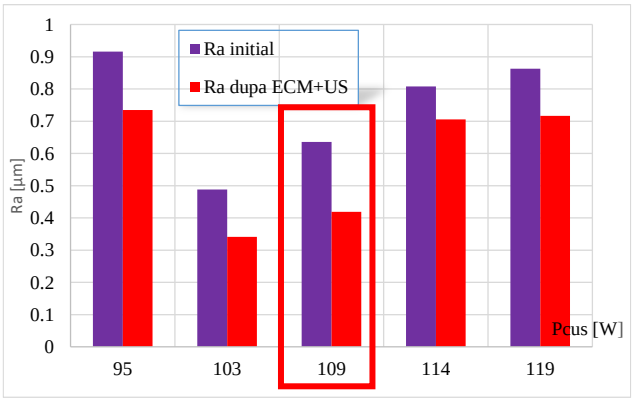

Figure 33. Variation of Ra as a function of ultrasonic power P_{cus}

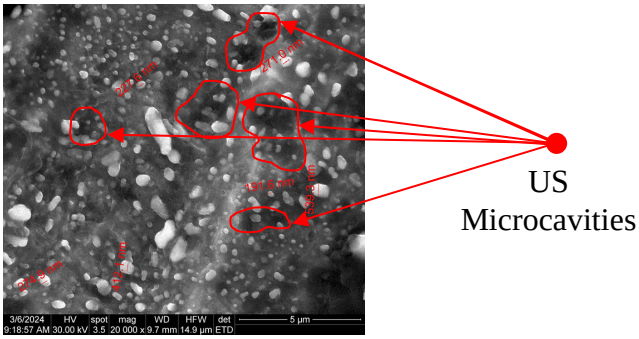

Figure 34. SEM image of the machined surface

10. CONCLUSIONS

The contributions of the study are: numerical simulation to obtain the eigenfrequency resonance condition of ultrasonic concentrators, integrating tools of different sizes with different electrical insulating layer thicknesses, used to assist ECM polishing; numerical simulation of Fe2O3 layer depassivation and ultrasonic material removal in ultrasonic-assisted ECM polishing of 12% Cr stainless steel; validation of the models obtained by numerical simulation by experimental data showing the correct operation of the ultrasonic chains and finding an optimum US generator power for maximum roughness decrease after a single cycle of operation.

Future research directions are: modelling material removal by introducing submicrometric Cr carbide particles, which influence the process; improving the experimental stand by adjusting the frequency range of the US generator and adaptive control to maintain the resonant frequency during processing; correlating US removal with ECM by repeating the operating cycle and further reducing the roughness of the machined surface.

11. REFERENCES

[1]. El-Hofy, H., *Vibration-assisted electrochemical machining: a review*, The International Journal of Advanced Manufacturing Technology, ISSN 0268-3768, (2019).

[2]. Ghiculescu, D., Contributions to Development and Innovation of Ultrasonically Aided Nonconventional Machining, Teză de abilitare, UPB 2016.

[3]. Rajkumar, K.P., Poovazhagan, L. Saravanamuthukumar, P. Javed Syed Ibrahim S, Santosh S., *Abrasive assisted electrochemical machining of Al-B4C nanocomposite*, Appl. Mech. Mater. 787:523-527, (2015).

[4]. Davydov A.D, Volgin V.M., Lyubimov V.V., *Electrochemical machining of metals: fundamentals of electrochemical shaping*, Russ. J. Electrochem. 40(12):1230–1265, (2004).

[5]. Rajurkar, K.P., Kozak, J, Wei B, McGeough JA, *Study of pulse electrochemical machining characteristics*, CIRP Ann. Manuf. Technol. 42(1):231-234, (1993).

[6]. Jigar B. Patel, Zhujian Feng, et. al., *Quality Enhancement with Ultrasonic Wave and Pulsed Current in Electrochemical Machining*, Procedia Manufacturing, ISSN 2351-9789, (2017).

[7]. Nicoară, Dan, Hedes, Alexandru, Şora, Ioan, *Ultrasonic enhancement of an electrochemical machining process*, Universitatea Politehnica din Timișoara 5. 213-218, (2006).

[8]. Skoczypiec, Sebastian, *Research on ultrasonically assisted electrochemical machining process*, The International Journal of Advanced Manufacturing Technology. 52. 565-574. 10.1007/s00170-010-2774-4, (2011).

[9]. Liu, Jia, Liu, Yan, Zhang, Zhe, Wang, Hao, *Parameter Optimization and Experimental Study on Tool-Vibration-Assisted Pulsed Electrochemical Machining of γ-TiAl TNM Blades*, Applied Sciences. 12. 8042, (2022).

[10]. Xiangming, Z. Yong, L. Jianhua, Z. Kan, W. Huanhgai, K., *Ultrasonic-assisted electrochemical drill-grinding of small holes with high-quality*, Journal of Advanced Research, ISSN 2090-1232, (2020).

[11]. Yongcheng, G. Wangwang, C. Yongwei, Z., *Experimental Study on Ultrasonic Assisted Electrochemical Micro-Machining of Micro-Dimple Array Structure*, International Journal of Electrochemical Science, ISSN 1452-3981, (2021).

[12]. Singh, Tarlochan, *Experimental investigations of energy channelization behavior in ultrasonic assisted electrochemical discharge machining*, Journal of Materials Processing Technology, 293: 117084, (2021).

[13]. Drobota, V., Rezistenta materialelor, Editura tehnica, (1982).

[14]. A. Ouglova, Y. Berthaud, M. François, F. Foct, *Mechanical properties of an iron oxide formed by corrosion in reinforced concrete structures*, Corrosion Science, Volume 48, Issue 12, p. 3988-4000, (2006).

[15]. Hassan, E.H., Vibration-assisted electrochemical machining: a review, The International Journal of Advanced Manufacturing Technology, Vol. 105, p. 579-593, (2019).

[16]. Saxena, K.K., Qian, J., Reynaerts, D., A review on process capabilities of electrochemical micromachining and its hybrid variants, International Journal of Machine Tools and Manufacture, Vol. 127, p. 28-56, (2018).

[17]. Zhang, Y., Investigation Into Current Efficiency For Pulse Electrochemical Machining Of Nickel Alloy, Industrial and Management Systems Engineering, M.S. Thesis, University of Nebraska - Lincoln, (2010).